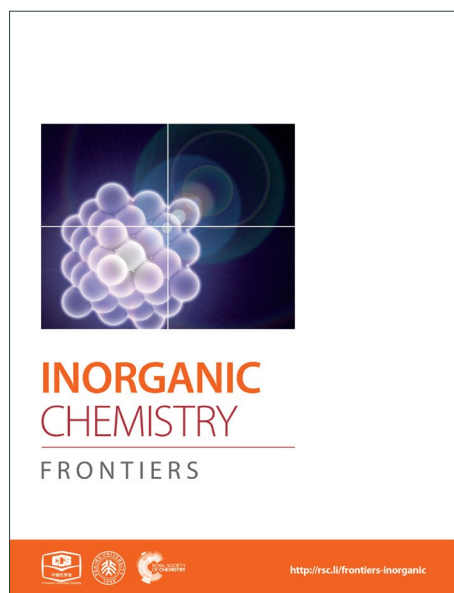
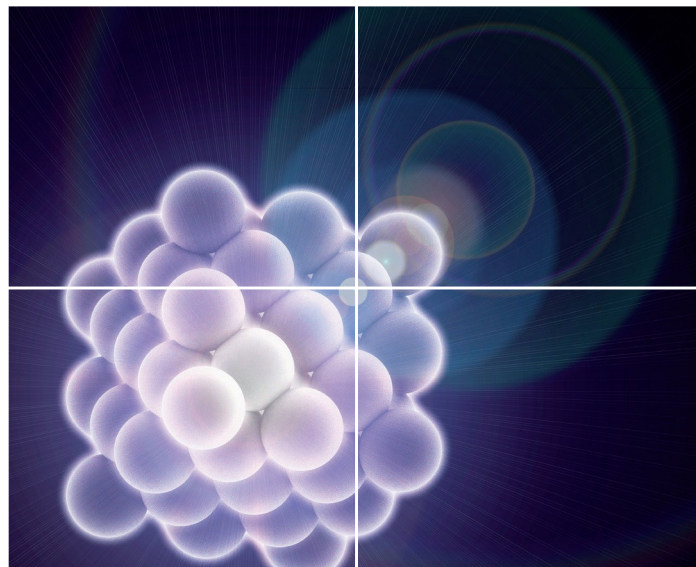


# INORGANIC CHEMISTRY

FRONTIERS

Accepted Manuscript



This is an *Accepted Manuscript*, which has been through the Royal Society of Chemistry peer review process and has been accepted for publication.

*Accepted Manuscripts* are published online shortly after acceptance, before technical editing, formatting and proof reading. Using this free service, authors can make their results available to the community, in citable form, before we publish the edited article. We will replace this *Accepted Manuscript* with the edited and formatted *Advance Article* as soon as it is available.

You can find more information about *Accepted Manuscripts* in the [Information for Authors](#).

Please note that technical editing may introduce minor changes to the text and/or graphics, which may alter content. The journal's standard [Terms & Conditions](#) and the [Ethical guidelines](#) still apply. In no event shall the Royal Society of Chemistry be held responsible for any errors or omissions in this *Accepted Manuscript* or any consequences arising from the use of any information it contains.



Journal Name

COMMUNICATION

## MoS<sub>2</sub> with intercalation reaction as long-life anode material for Lithium ion batteries

Received 00th January 20xx,  
Accepted 00th January 20xx

Zhe Hu<sup>a</sup>, Qiannan Liu<sup>a</sup>, Weiyi Sun<sup>b</sup>, Weijie Li<sup>a</sup>, Zhanliang Tao<sup>\*,a,b</sup>, Shu-Lei Chou<sup>\*,a</sup>, Jun Chen<sup>b,c</sup>, and Shi-Xue Dou<sup>a</sup>

DOI: 10.1039/x0xx00000x

www.rsc.org/

**MoS<sub>2</sub> with expanded layers were synthesized and characterized as anode materials for lithium ion batteries in ether-based electrolyte by cutting off the terminal discharge voltage to 1.0 V to keep MoS<sub>2</sub> away from conversion reaction. The as-prepared MoS<sub>2</sub> achieved 96% of capacity retention even after 1400 cycles and showed good performances in full cell with LiCoO<sub>2</sub> as the counter electrode.**

Recently rechargeable batteries have attracted large amount attentions mainly because of their cyclability as sustainable power supply.<sup>1-3</sup> Especially for the rechargeable lithium ion batteries (LIBs), the practical applications mostly facilitate the social development.<sup>4, 5</sup> Among different kinds of electrode materials, MoS<sub>2</sub> has become one of the most popular materials owing to the layered structure like graphite.<sup>6-8</sup> The weak van der Waals force between the adjacent layers is easy to be broken by lithium ion insertion and the fully transition reaction will provide a high specific capacity of 670 mAh·g<sup>-1</sup> (four-electron reaction).<sup>9-11</sup> In order to get the optimized electrochemical performances, the reaction mechanism of MoS<sub>2</sub> cycling in 0.1–3.0 V has been widely discussed.<sup>12, 13</sup> At the first cycle, there is an intercalation process for MoS<sub>2</sub> reacting with Li<sup>+</sup> to form LiMoS<sub>2</sub>, which accompanies the phase change from MoS<sub>2</sub> with trigonal pristine (2H-MoS<sub>2</sub>) to trigonal antiprismatic MoS<sub>2</sub>(1T-MoS<sub>2</sub>).<sup>10</sup> As the interlayer spacing is much larger than graphite, it will introduce less volume change regarding the intercalation process.<sup>14</sup> Then with continuous Li<sup>+</sup> intercalation, the structure of layered MoS<sub>2</sub> decomposes to Mo metal and Li<sub>2</sub>S. This step possesses large volume expansion (~103%) leading to electrode pulverization.<sup>15-17</sup> Because the charge products can never return back to MoS<sub>2</sub> again, the

reaction mechanism of the following cycles is the reversible reaction between Li<sub>2</sub>S and S, just the same as Li/S batteries. Here comes the problem that MoS<sub>2</sub> should also come across the difficulties as those in Li/S batteries, such as the severe capacity loss owing to the active materials dissolution, polysulfide shuttling effect, and side reaction between polysulfides and electrolyte.<sup>18-20</sup> So it is urgent to find proper method to solve the problems mentioned above.

The most effective method is the nano-size design together with carbon modification.<sup>21</sup> The nano-size design would provide short ion diffusion path, which will enhance the reaction kinetics.<sup>22</sup> By coating with carbon, the active materials can be protected from the negative effect of the volume expansion and accelerate the surface electron transportation. Qiao and coworkers synthesized mesoporous MoS<sub>2</sub> with expanded interlayer. The as-prepared product showed an initial capacity of 1052 mAh·g<sup>-1</sup> and lasted for 100 cycles at 0.1 A·g<sup>-1</sup>.<sup>18</sup> Although carbon coating leads great improvement on the MoS<sub>2</sub>/Li batteries, the cycling performance is still hard to match the need for commercialization, and the broaden voltage region (0.1–3.0 V) still suffers from safety issues like electrolyte decomposition, large volume change (203% after change), and precipitation of lithium metal on the anode surface of LIBs. Thus to further improve the electrochemical performance of MoS<sub>2</sub>, there should be more modification beside carbon coating and nano-size design.

According to previous work on MoS<sub>2</sub>, FeS<sub>2</sub> and FeSe<sub>2</sub>, setting proper cut-off voltage to prevent a conversion type reaction happening is an effective way to improve the cycling life.<sup>23-25</sup> Py et al. has excluded the possibility for lithium/electrolyte co-intercalation.<sup>26</sup> After lithium intercalating there is only 0.14 Å expanded for the MoS<sub>2</sub> interlayer. And the intercalation reaction can confine the charge and discharge platform mainly locating in the voltage range of 1.5–2.0 V. So it is a prominent improvement on the volume and voltage control for intercalation reaction than the conversion type reaction. This inspires us to fabricate the full cell using MoS<sub>2</sub> as anode material mainly because the low volume change and high terminal discharge voltage just like Li<sub>4</sub>Ti<sub>5</sub>O<sub>12</sub>, etc.<sup>16, 27</sup> As

<sup>a</sup>Institute for Superconducting and Electronic Materials  
Australian Institute for Innovative Materials  
University of Wollongong, Innovation Campus  
Squires Way, North Wollongong NSW 2522, Australia

<sup>b</sup>Key Laboratory of Advanced Energy Materials Chemistry (Ministry of Education),  
Nankai University, Tianjin, 300071, People's Republic of China.

<sup>c</sup>Collaborative Innovation Center of Chemical Science and Engineering, Nankai  
University, Tianjin, 300071, People's Republic of China

Electronic Supplementary Information (ESI) available: [Experimental Section, XRD, TEM, and electrochemical characterization]. See DOI: 10.1039/x0xx00000x

known, the high-voltage cathode materials (e.g.  $\text{LiCoO}_2$  and  $\text{LiNi}_{0.5}\text{Mn}_{1.5}\text{O}_4$ ) that always suffer from the risk of electrolyte decomposition when charging over 4.0 V in the practical use. Fig. 1 shows the typical charge and discharge curves of cathode material  $\text{LiCoO}_2$ , and anode materials  $\text{MoS}_2$ ,  $\text{Li}_4\text{Ti}_5\text{O}_{12}$ , and graphite. Graphite is the most popular commercial anode material owing to its cheap price, relative stable cyclability, and competitive specific capacity. However the charge and discharge curves are almost around 0 V, which probably leads to the deposition of lithium metal on the surface of anode materials and then causes severe safety issues like short circuit. But materials such as  $\text{MoS}_2$  and  $\text{Li}_4\text{Ti}_5\text{O}_{12}$ , which hold much safer voltage region from 1.0–3.0 V (half cell), can not only avoid safety issues like short circuit and large volume change during cycling (full cell) but also lower risk for electrolyte decomposition when served as the counter electrode of high voltage cathode material.<sup>14, 28</sup> Nevertheless, until now there are only a few papers focusing on the  $\text{MoS}_2/\text{Li}$  battery with intercalation reaction.<sup>26, 29-31</sup>

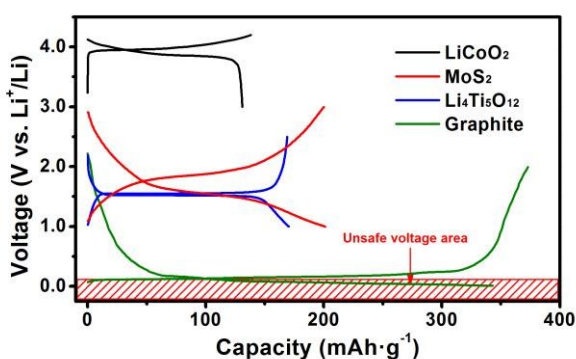


Fig. 1 The typical charge and discharge curves of  $\text{LiCoO}_2$ ,  $\text{MoS}_2$ ,  $\text{Li}_4\text{Ti}_5\text{O}_{12}$ , and graphite.

Herein we have synthesized the  $\text{MoS}_2$  with expanded layers (H- $\text{MoS}_2$ ) through hydrothermal process and freeze-drying method by modifying the experimental method of our previous work.<sup>23</sup> To preserve the layer structure, obtain relative high specific capacity and protect the electrolyte from decomposition, the terminal discharge voltage was set to 1.0 V. The stable charge and discharge platform was  $\sim 1.8$  V and  $\sim 1.6$  V, which ensured the possible applications for commercial rechargeable lithium batteries and anode in rechargeable LIBs (full cell with  $\text{LiCoO}_2$  as the counter electrode).

The H- $\text{MoS}_2$  represents the product procured by hydrothermal treatment, and B- $\text{MoS}_2$  represents the bulk  $\text{MoS}_2$  purchased from (Alfa aesar, 10–20  $\mu\text{m}$ ). Fig. S1a illustrates the X-ray diffraction (XRD) patterns of H- $\text{MoS}_2$  and B- $\text{MoS}_2$ . Results show that the H- $\text{MoS}_2$  shows broadening characteristic peaks, and lower peak intensity. On the contrary, B- $\text{MoS}_2$  holds the sharp and strong XRD peaks. Meanwhile the peak shift of the (002) crystal plane indicates the layers in H- $\text{MoS}_2$  slightly expand. Fig. S1b and S1c depict the high resolution transmission electron microscopy (HRTEM) images of H- $\text{MoS}_2$  and B- $\text{MoS}_2$ . The d-spacing calibrated from the crystal fringes is in accordance with the XRD analysis: H- $\text{MoS}_2$  layers (layer

distance of 0.69 nm) arrange disordered and rich-defective, however the B- $\text{MoS}_2$  possesses the neatly restack  $\text{MoS}_2$  layers with the d-spacing of 0.62 nm. Through the freeze-drying process, which is also used as the most effective way to fabricate 2D/3D graphene, the ice plays an important role in supporting the morphology.<sup>32</sup> When the ice is evacuated from the powders, the  $\text{MoS}_2$  layers with expanded space can preserve. Then the electrochemical performances were tested. Fig. 2a and Fig. S2a exhibit the galvanostatic charge and discharge curves of H- $\text{MoS}_2$  and B- $\text{MoS}_2$  at  $0.2 \text{ A}\cdot\text{g}^{-1}$ . Referring to the initial cycle, the H- $\text{MoS}_2$  has higher discharge platform ( $\sim 1.5$  V) and more specific discharge capacity ( $260 \text{ mAh}\cdot\text{g}^{-1}$ ) than B- $\text{MoS}_2$  ( $\sim 1.1$  V and  $181 \text{ mAh}\cdot\text{g}^{-1}$ ) because of the different d-spacing of (002). Larger layer distance facilitates the kinetics of  $\text{Li}^+$  intercalation leading to smaller energy barrier and the stable thermodynamics expressing as the stronger capacity for accommodating more  $\text{Li}^+$ .<sup>33, 34</sup> From the cyclic data (Fig. 2b and Fig. S2b), The capacities at 2nd cycle reveal a slight decrease and the detailed values are 195 and  $108 \text{ mAh}\cdot\text{g}^{-1}$  of H- $\text{MoS}_2$  and B- $\text{MoS}_2$ , respectively, which should be ascribed to the partial side reaction and the possibility for trace residual  $\text{Li}^+$  inside the layers. Then the discharge capacity has become a little higher ( $5\text{--}10 \text{ mAh}\cdot\text{g}^{-1}$ ), which is resulted from the activation for the electrode materials.<sup>10</sup> What's more, after 1st cycle the charge and discharge curves changes a bit. As the mechanism of the 1st discharge process is well investigated. It should be the phase conversion from  $\text{MoS}_2(2\text{H})$  to  $\text{MoS}_2(1\text{T})$ , which is the main reason for the curve changes.<sup>26</sup> Fig. 2b reveals the cyclic performance of the H- $\text{MoS}_2$ . After 1st cycle, the specific charge/discharge capacities are around  $190 \text{ mAh}\cdot\text{g}^{-1}$ . And then with gradual activation, the specific capacity keeps stable at  $205 \text{ mAh}\cdot\text{g}^{-1}$  and after 1400 cycles the capacity retention is 96% (compared to the capacity of the second cycle). The coulombic efficiency suffers a low value at 1st cycle (75%) and then gradually increases to near 100% and be stable for 1400 cycles. Fig. 2c shows the rate property of H- $\text{MoS}_2$ . The discharge capacities at 0.2, 1, 2, and  $3 \text{ A}\cdot\text{g}^{-1}$  are 200, 115, 70, 50  $\text{mAh}\cdot\text{g}^{-1}$ , respectively. H- $\text{MoS}_2$  displays high capacity at low current density, and considerable capacity at  $1 \text{ A}\cdot\text{g}^{-1}$ . The H- $\text{MoS}_2$  battery can perform well recover capability for the high current density treatment: the discharge capacity can return back to  $200 \text{ mAh}\cdot\text{g}^{-1}$  at  $0.2 \text{ A}\cdot\text{g}^{-1}$  after treating with  $3 \text{ A}\cdot\text{g}^{-1}$ .

The half cell performance at  $0.2 \text{ A}\cdot\text{g}^{-1}$  in the voltage range of 0.1–3 V was also tested (Fig. S2c and S2d). As expected, the large voltage polarization between the charge and discharge process proves the above analysis that it is not suitable for full cell use. Although the discharge capacity can reach  $670 \text{ mAh}\cdot\text{g}^{-1}$  (4 electrons/  $\text{Li}^+$  ions reaction), the large volume change generating from the formation of conversion product Mo and  $\text{Li}_2\text{S}$  leads to the capacity fade and worse reaction kinetics, which is proved by the GITT characterization (Fig. S3 and S4). It is clear that after the first discharge process, the H- $\text{MoS}_2$  battery cycling between 0.1–3.0 V shows sluggish ion diffusion (the lithium diffusion coefficient decrease almost 1–2 order of magnitude) leading to the large voltage polarization (Fig. S3b). However the H- $\text{MoS}_2$  battery cycling from 1.0 to

3.0 V possesses a fast lithium migration ( $\sim 10^{-9} \text{ cm}^2 \cdot \text{s}^{-1}$ ) ensuring the stable electrochemical performances mentioned above. The ester-based electrolyte (ethylene carbonate and diethyl carbonate) is used to investigate influence of the electrolyte. As shown in Fig. S4, the  $\text{Li}/\text{MoS}_2$  cell also performs well cycling stability. According to the above analysis, it means that the cut-off voltage is the most important reason for achieving long life.

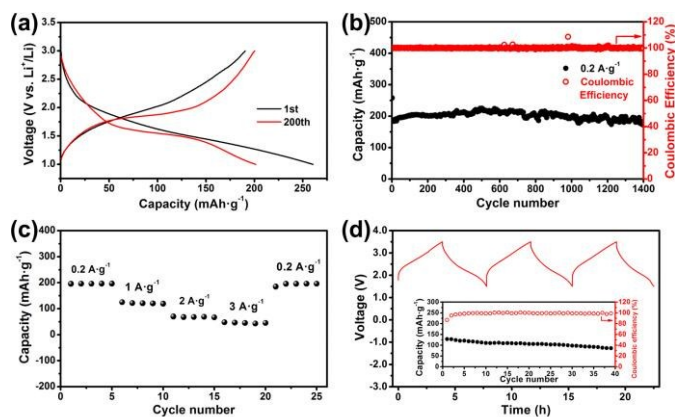


**Fig. 2** Electrochemical performances of the as-prepared  $\text{MoS}_2$  and the full cell assembled by  $\text{LiCoO}_2$  as cathode and  $\text{MoS}_2$  as anode. (a) Galvanostatic charge and discharge curves of  $\text{MoS}_2$  at 1st and 200th cycles at a current density of  $0.2 \text{ A} \cdot \text{g}^{-1}$ . (b) Cyclic performance and (c) rate property of  $\text{MoS}_2$ . (d) Galvanostatic charge and discharge curves of the full cell at the voltage range from 1.5–3.5 V (inset is the cyclic performance).

To further investigate the possibility of using as anode material, we have fabricated the full cell using  $\text{LiCoO}_2$  as cathode material and  $\text{H-MoS}_2$  as anode material. The electrochemical performances of the assembled full cell are estimated by the active mass of cathode material and are tested under 0.1C ( $14 \text{ mA} \cdot \text{g}^{-1}$ ). The galvanostatic charge and discharge curves are shown in Fig. 2d. The average charge platform is  $\sim 2.80 \text{ V}$  and average discharge platform is  $\sim 2.35 \text{ V}$ . The slope of discharge platform is convenient and accurate for the residual capacity indication. The cyclic data inserted in Fig. 2d shows that the 1st discharge capacity is  $120 \text{ mAh} \cdot \text{g}^{-1}$  with a coulombic efficiency of 82%. Then the coulombic efficiency improves to near 99% along with the capacity loss from 120 to  $90.5 \text{ mAh} \cdot \text{g}^{-1}$ . Graphite/ $\text{LiCoO}_2$  full cell is also performed (Fig. S5). The charge and discharge platforms are at 4.0 and 3.6 V, respectively and the discharge capacity is  $132 \text{ mAh} \cdot \text{g}^{-1}$ . After cycling for 30 times, the capacity retention is 91.6%. Thus the performance of  $\text{MoS}_2/\text{LiCoO}_2$  battery is comparable with that of commercial type graphite/ $\text{LiCoO}_2$  battery, and moreover  $\text{MoS}_2$  possesses higher safety factor because of its high charge and discharge voltage region (Fig. 1). The full cell technology should be improved in further investigations such as to design high tapping density  $\text{MoS}_2$  with high electrochemical performances. However this result shows the possibility for  $\text{MoS}_2$  using as anode material for LIBs.

The electrochemical impedance spectroscopy (EIS) measurement of  $\text{H-MoS}_2$  at different voltage range was also characterized (Fig. S7). Both EIS data in 1.0–3.0 V and 0.1–3.0 V exhibit one circle at high frequency and a line at low

frequency. Comparing the different voltage range, the charge transfer resistance of intercalation reaction is much smaller than that of conversion reaction. Moreover the  $\text{H-MoS}_2$  shows smaller charge transfer resistance than  $\text{B-MoS}_2$ , resulting from the better nano-design that facilitates the electrochemical reaction kinetics.

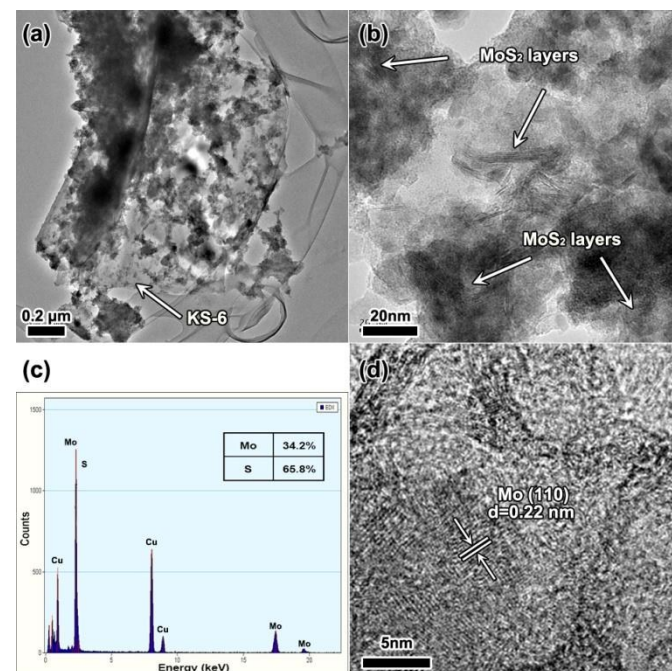


**Fig. 3** TEM characterization of the electrode material (half cell) after cycling. (a) The TEM image, (b) HRTEM image, and (c) EDX of  $\text{MoS}_2$  electrode at 1.0 V after cycling between 1.0 V and 3.0 V for 100 times. (d) HRTEM image of  $\text{MoS}_2$  electrode at 0.1 V after cycling at 0.1–3.0 V for 10 times.

Fig. 3 shows the further investigations on the electrode material after cycling. The transmission electron microscopy (TEM) and HRTEM images of  $\text{MoS}_2$  electrode after cycling for 100 times are shown in Fig. 3a and 3b. It is noticed that the graphite (conductive additive, KS-6) is served as the carrier for the  $\text{MoS}_2$  particles and as the conductive substrate between the collector and  $\text{MoS}_2$  particles. We also find the  $\text{MoS}_2$  layers preserved after cycling, which means that the conversion reaction does not happen when the terminal discharge voltage is set to 1.0 V. The energy dispersive X-ray spectroscopy (EDX) measurement is also employed to detect the elemental content of Mo and S. The result shows that the atom ratio of Mo versus S is about 1:2, but still the S has proved to be loss about 2%, which should be ascribed to the systematic error and the partial over-discharge effect. Fig. 3d reveals the electrode material cycling for 10 times in the voltage range of 0.1–3.0 V. Apparently nano-sized Mo particles are detected and found to be a little aggregated, which would cause the separation for the Mo and  $\text{Li}_2\text{S}$  leading to a severe capacity loss.<sup>16</sup>

The overall characterization and discussion connect together the proofs of the excellent electrochemical properties of  $\text{H-MoS}_2$  cycling in 1.0–3.0 V. The expanded layers provide better thermodynamic and kinetics, expressing as the higher discharge voltage and fast ionic conductivity. Eliminating the conversion reaction, the wholly preserved layer-structured  $\text{MoS}_2$  ensures

the rechargeable ability for the MoS<sub>2</sub>/Li and LiCoO<sub>2</sub>/MoS<sub>2</sub> batteries. The smaller charge transfer resistance reveals the improved kinetics leading to the smaller voltage polarization.

## Conclusions

The as-prepared MoS<sub>2</sub> were synthesized through the hydrothermal process. By cutting off the terminal discharge voltage to 1.0 V in ether-based electrolyte, H-MoS<sub>2</sub> exhibits a high discharge capacity of 200 mAh·g<sup>-1</sup> at 0.2 A·g<sup>-1</sup> with a stable charge and discharge platform of ~1.8 V and ~1.6 V, respectively. Referring the cyclability, it can cycle for 1400 times with almost no capacity fade. Thus to control the terminal discharge voltage should be an effective way to improve conversion type materials with two key factors that own an intercalation process before the conversion reaction happens and easy-control voltage management. More attentions should focus on the intercalation reaction so that MoS<sub>2</sub> would finally find promising applications as the anode material for rechargeable lithium ion batteries.

## Acknowledgement

This work is financially supported by the Australian Research Council (ARC) through a Linkage Project (LP120200432) and the Commonwealth of Australia through the Automotive Australia 2020 Cooperative Research Centre (Auto CRC). The authors acknowledge use of the facilities at the UOW Electron Microscopy Centre funded by ARC grants (LE0882813 and LE0237478). The authors would also like to thank Dr. Tania Silver for critical reading of the manuscript.

## Notes and references

‡ Footnotes relating to the main text should appear here. These might include comments relevant to but not central to the matter under discussion, limited experimental and spectral data, and crystallographic data.

- B. Dunn, H. Kamath and J.-M. Tarascon, *Science*, 2011, **334**, 928-935.
- K. Kang, Y. S. Meng, J. Bréger, C. P. Grey and G. Ceder, *Science*, 2006, **311**, 977-980.
- H. J. Yu, Y. Ren, D. D. Xiao, S. H. Guo, Y. B. Zhu, Y. M. Qian, L. Gu and H. S. Zhou, *Angew. Chem. Int. Ed.*, 2014, **53**, 8963-8969.
- Y. Sun, J. Zhu, L. Bai, Q. Li, X. Zhang, W. Tong and Y. Xie, *Inorg. Chem. Front.*, 2014, **1**, 58-64.
- S. Xu, S. Lau and L. A. Archer, *Inorg. Chem. Front.*, 2015, DOI: 10.1039/c1035qi00169b.
- J. Zhou, J. Qin, X. Zhang, C. Shi, E. Liu, J. Li, N. Zhao and C. He, *ACS nano*, 2015, **9**, 3837-3848.
- R. Tenne, *Nat. Nanotech.*, 2006, **1**, 103-111.
- X. Huang, Z. Y. Zeng and H. Zhang, *Chem. Soc. Rev.*, 2013, **42**, 1934-1946.
- X. Cao, Y. Shi, W. Shi, X. Rui, Q. Yan, J. Kong and H. Zhang, *Small*, 2013, **9**, 3433-3438.
- H. Hwang, H. Kim and J. Cho, *Nano Lett.*, 2011, **11**, 4826-4830.
- K. Chang and W. X. Chen, *J. Mater. Chem.*, 2011, **21**, 17175-17184.
- J. Xiao, X. J. Wang, X. Q. Yang, S. D. Xun, G. Liu, P. K. Koech, J. Liu and J. P. Lemmon, *Adv. Funct. Mater.*, 2011, **21**, 2840-2846.
- P. Sun, W. Zhang, X. Hu, L. Yuan and Y. Huang, *J. Mater. Chem. A*, 2014, **2**, 3498-3504.
- Z. Wu, B. Li, Y. Xue, J. Li, Y. Zhang and F. Gao, *J. Mater. Chem. A*, 2015, **3**, 19445-19454.
- Y. Gong, S. Yang, Z. Liu, L. Ma, R. Vajtai and P. M. Ajayan, *Adv. Mater.*, 2013, **25**, 3979-3984.
- T. Stephenson, Z. Li, B. Olsen and D. Mitlin, *Energy Environ. Sci.*, 2014, **7**, 209-231.
- Y. X. Wang, S. L. Chou, D. Wexler, H. K. Liu and S. X. Dou, *Chem. Eur. J.*, 2014, **20**, 9607-9612.
- H. Liu, D. Su, R. Zhou, B. Sun, G. Wang and S. Z. Qiao, *Adv. Energy Mater.*, 2012, **2**, 970-975.
- J. Gao, M. A. Lowe, Y. Kiya and H. D. Abruña, *J. Phys. Chem. C*, 2011, **115**, 25132-25137.
- Y.-X. Yin, S. Xin, Y.-G. Guo and L.-J. Wan, *Angew. Chem. Int. Ed.*, 2013, **52**, 13186-13200.
- C. B. Zhu, X. K. Mu, P. A. van Aken, Y. Yu and J. Maier, *Angew. Chem. Int. Ed.*, 2014, **53**, 2152-2156.
- K. Zhang, X. Han, Z. Hu, X. Zhang, Z. Tao and J. Chen, *Chem. Soc. Rev.*, 2014.
- Z. Hu, L. Wang, K. Zhang, J. Wang, F. Cheng, Z. Tao and J. Chen, *Angew. Chem. Int. Ed.*, 2014, **53**, 12794-12798.
- Z. Hu, Z. Zhu, F. Cheng, K. Zhang, J. Wang, C. Chen and J. Chen, *Energy Environ. Sci.*, 2015, **8**, 1309-1316.
- K. Zhang, Z. Hu, X. Liu, Z. Tao and J. Chen, *Adv. Mater.*, 2015, **27**, 3305-3309.
- M. A. Py and R. R. Haering, *Can. J. Phys.*, 1983, **61**, 76-84.
- Z. Hu, K. Zhang, Z. Zhu, Z. Tao and J. Chen, *J. Mater. Chem. A*, 2015, **3**, 12898-12904.
- Z. Zhu, F. Cheng and J. Chen, *J. Mater. Chem. A*, 2013, **1**, 9484-9490.
- N. Imanishi, K. Kanamura and Z. i. Takehara, *J. Electrochem. Soc.*, 1992, **139**, 2082-2087.
- C. Julien, S. I. Saikh and G. A. Nazri, *Mater. Sci. Eng. B*, 1992, **15**, 73-77.
- Y. Miki, D. Nakazato, H. Ikuta, T. Uchida and M. Wakihara, *J. Power Sources*, 1995, **54**, 508-510.
- L. Qian and H. Zhang, *J. Chem. Technol. Biotechnol.*, 2011, **86**, 172-184.
- K. Chang, W. Chen, L. Ma, H. Li, H. Li, F. Huang, Z. Xu, Q. Zhang and J.-Y. Lee, *J. Mater. Chem.*, 2011, **21**, 6251-6257.
- S. Q. Yang, D. X. Li, T. R. Zhang, Z. L. Tao and J. Chen, *J. Phys. Chem. C*, 2011, **116**, 1307-1312.